

Activity-Independent Prespecification of Synaptic Partners in the Visual Map of *Drosophila*

P. Robin Hiesinger, R. Grace Zhai, Yi Zhou, Tong-Wey Koh, Sunil Q. Mehta, Karen L. Schulze, Yu Cao, Patrik Verstreken, Thomas R. Clandinin, Karl-Friedrich Fischbach, Ian A. Meinertzhagen, and Hugo J. Bellen

Supplemental Experimental Procedures

Tetrodotoxin Injection, Rearing of Temperature-Sensitive *para^{ts1}* Pupae and Activity Mutants

To achieve development under conditions of blockade of voltage-sensitive sodium channels, we used two approaches: tetrodotoxin injection (TTX [ICN Biomedicals, Inc., OH]) and analysis of the sodium channel mutant *para^{ts1}* [S1]. For TTX injections, we removed the top of the pupal case above the head from 40–50 wild-type pupae at P+25% and 30 at P+50% as well as the same number of pupae for control injections. Either 10 mM TTX [S2] or distilled water was injected through the eye into the optic lobe with an Eppendorf Transjector 5246 microinjection machine. The pupae were then allowed to develop in a humid chamber at 25°C to become pharate adults. In a first experiment, TTX injections at P+25% were performed. Of 33 TTX-injected specimens that developed to adulthood, none eclosed. Of 39 controls that developed to adulthood, 25 eclosed. In a second experiment with injections at P+50%, of 20 TTX-injected specimens that developed to adulthood, none eclosed, whereas in the control, 14 of 23 eclosed. These experiments show that development continues despite the TTX injection, but leave the pupa unable to eclose. The animals were dissected as either pharate or newly eclosed adults and stained with mAb 24B10 (anti-Chaoptin).

Prolonged exposure of *para^{ts1}* mutant pupae to restrictive temperatures is lethal; developmental experiments with such pupae were therefore performed in a PCR machine (Stratagene Robocycler) with a temperature cycle of 22°C for 30 min (permissive) followed by 90 min at 32°C (restrictive) for 50–75 hr in humid chambers; wild-type pupae were used as controls under the same conditions. Late pupae and eclosed adults were stained with mAbs 24B10.

syt^{AD4} mutants are embryonic or larval lethal [S3]. To analyze *syt* mutant visual maps, we selectively rendered the visual system mutant [S4, S5]. Flies mutant for *inaC^{P209}*, *inaD^{P215}* [S6], *trp³⁴³*, *trpl³⁰²* [S7], *norPA^{P24}* [S8], or *hdc^{ik910}* [S9] are viable.

Supplemental References

- S1. Ganetzky, B. (1984). Genetic studies of membrane excitability in *Drosophila*: lethal interaction between two temperature-sensitive paralytic mutations. *Genetics* 108, 897–911.
- S2. Broadie, K., and Bate, M. (1993). Activity-dependent development of the neuromuscular synapse during *Drosophila* embryogenesis. *Neuron* 11, 607–619.
- S3. DiAntonio, A., Parfitt, K.D., and Schwarz, T.L. (1993). Synaptic transmission persists in synaptotagmin mutants of *Drosophila*. *Cell* 73, 1281–1290.
- S4. Newsome, T.P., Asling, B., and Dickson, B.J. (2000). Analysis of *Drosophila* photoreceptor axon guidance in eye-specific mosaics. *Development* 127, 851–860.
- S5. Stowers, R.S., and Schwarz, T.L. (1999). A genetic method for generating *Drosophila* eyes composed exclusively of mitotic clones of a single genotype. *Genetics* 152, 1631–1639.
- S6. Adamski, F.M., Zhu, M.Y., Bahiraei, F., and Shieh, B.H. (1998). Interaction of eye protein kinase C and INAD in *Drosophila*. Localization of binding domains and electrophysiological characterization of a loss of association in transgenic flies. *J. Biol. Chem.* 273, 17713–17719.
- S7. Niemeyer, B.A., Suzuki, E., Scott, K., Jalink, K., and Zuker, C.S. (1996). The *Drosophila* light-activated conductance is composed of the two channels TRP and TRPL. *Cell* 85, 651–659.
- S8. Bloomquist, B.T., Shorridge, R.D., Schneuwly, S., Perdew, M., Montell, C., Steller, H., Rubin, G., and Pak, W.L. (1988). Isolation of a putative phospholipase C gene of *Drosophila*, *norPA*, and its role in phototransduction. *Cell* 54, 723–733.
- S9. Burg, M.G., Sarthy, P.V., Koliantz, G., and Pak, W.L. (1993). Genetic and molecular identification of a *Drosophila* histidine decarboxylase gene required in photoreceptor transmitter synthesis. *EMBO J.* 12, 911–919.
- S10. Fujita, S., Zipursky, S., Benzer, S., Ferrus, A., and Shotwell, S. (1982). Monoclonal antibodies against the *Drosophila* nervous system. *Proc. Natl. Acad. Sci. USA* 79, 7929–7933.
- S11. Mehta, S.Q., Hiesinger, P.R., Beronja, S., Zhai, R.G., Schulze, K.L., Verstreken, P., Cao, Y., Zhou, Y., Tepass, U., Crair, M.C., et al. (2005). Mutations in *Drosophila sec15* reveal a function in neuronal targeting for a subset of exocyst components. *Neuron* 46, 219–232.
- S12. Richardt, A., Rybak, J., Stortkuhl, K.F., Meinertzhagen, I.A., and Hovemann, B.T. (2002). Ebony protein in the *Drosophila* nervous system: optic neuropile expression in glial cells. *J. Comp. Neurol.* 452, 93–102.
- S13. Hiesinger, P.R., Scholz, M., Meinertzhagen, I.A., Fischbach, K.F., and Obermayer, K. (2001). Visualization of synaptic markers in the optic neuropils of *Drosophila* using a new constrained deconvolution method. *J. Comp. Neurol.* 429, 277–288.
- S14. Clandinin, T.R., and Zipursky, S.L. (2000). Afferent growth cone interactions control synaptic specificity in the *Drosophila* visual system. *Neuron* 28, 427–436.
- S15. Verstreken, P., Koh, T.W., Schulze, K.L., Zhai, R.G., Hiesinger, P.R., Zhou, Y., Mehta, S.Q., Cao, Y., Roos, J., and Bellen, H.J. (2003). Synaptotagmin is recruited by endophilin to promote synaptic vesicle uncoating. *Neuron* 40, 733–748.

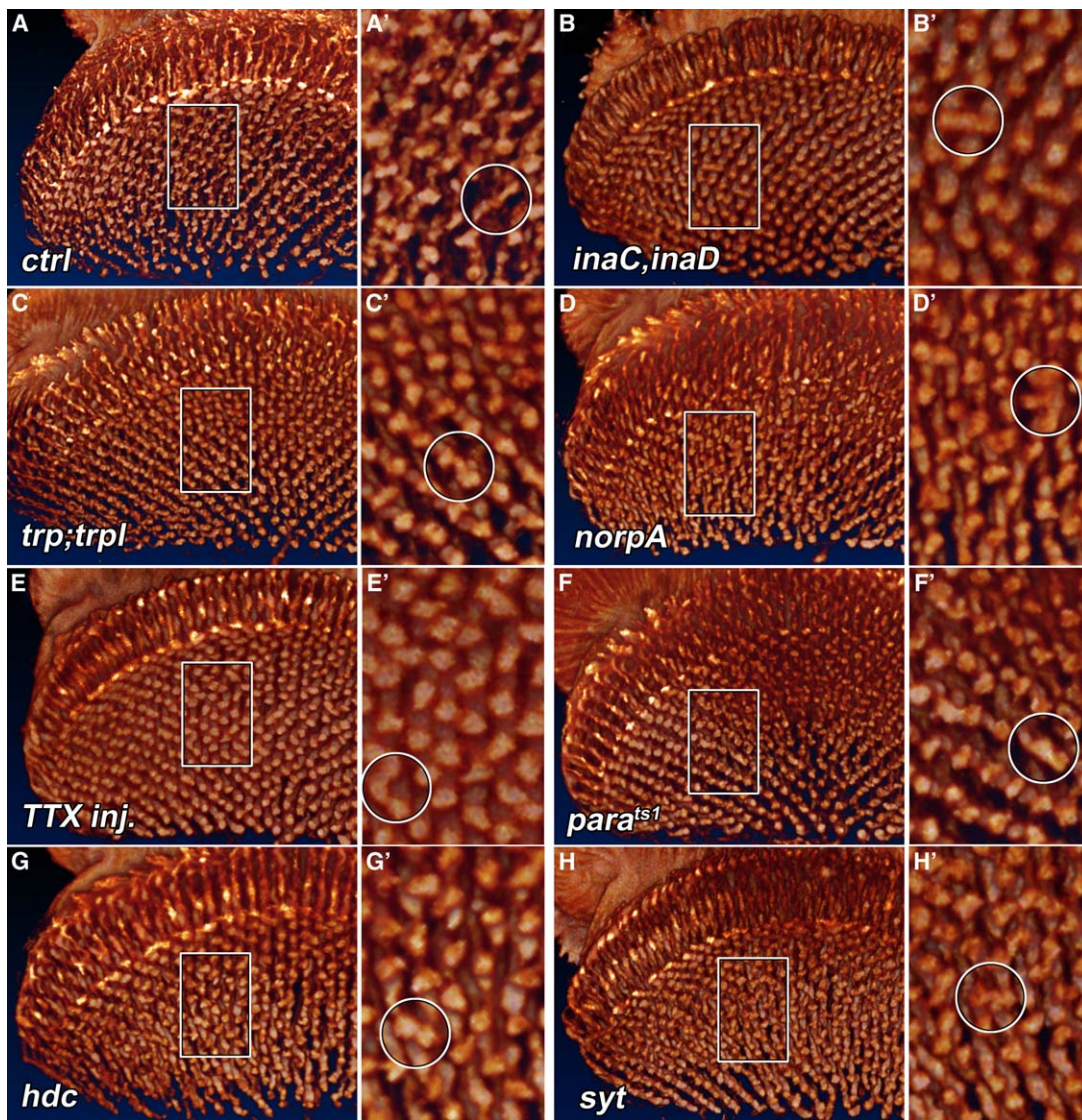


Figure S1. 3D Visualizations of R7 Projections in the Brain

(A) Control.

(B) *inaC^{p209}, inaD^{p215}* [S6].

(C) *trp³⁴³, trpl³⁰²* [S7].

(D) *norpA^{p24}* [S8].

(E) Injection of tetrodotoxin during development (TTX, see Supplemental Experimental Procedures).

(F) *para^{ts1}* [S1] after developmental heat-shock cycles (see Supplemental Experimental Procedures).

(G) *hdc^{k910}* [S9].

(H) *syt^{AD4}* [S3].

(A'–H') Enlarged views of the boxed areas in (A)–(H). R7 terminal fusions or filopodial overlaps are encircled. Box size: 20 × 30 μm. All specimens are labeled with anti-Chaoptin (mAb 24B10) [S10].

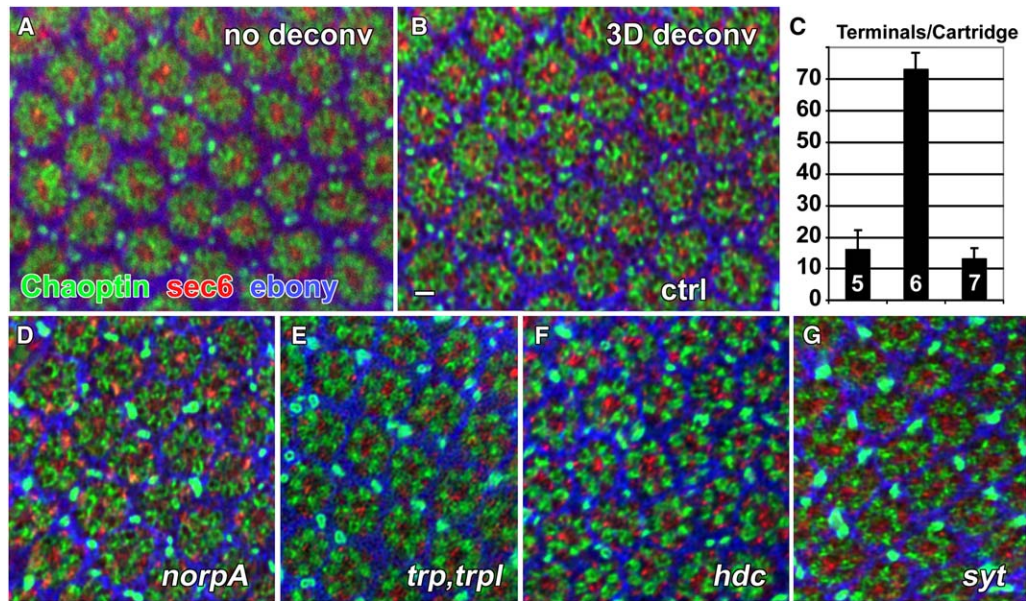


Figure S2. Confocal Microscopy on Lamina Cross-Sections of Activity Mutants

(A and B) All specimens are labeled with anti-Chaoptin (mAb 24B10) [S10] (green, R terminals), anti-Sec6 [S11] (red, postsynaptic cells), and anti-Ebony [S12] (blue, epithelial glia). Single confocal sections after blind deconvolution of 3D data sets [S13] are shown in all cases except (A), which is the original control picture before deconvolution as shown in (B).

(C) Distribution of terminals per cartridge averaged over all activity mutants. No significant difference was observed among the mutants and control. Scale bar in (B) represents 2 μ m for (A), (B), and (D)–(G).

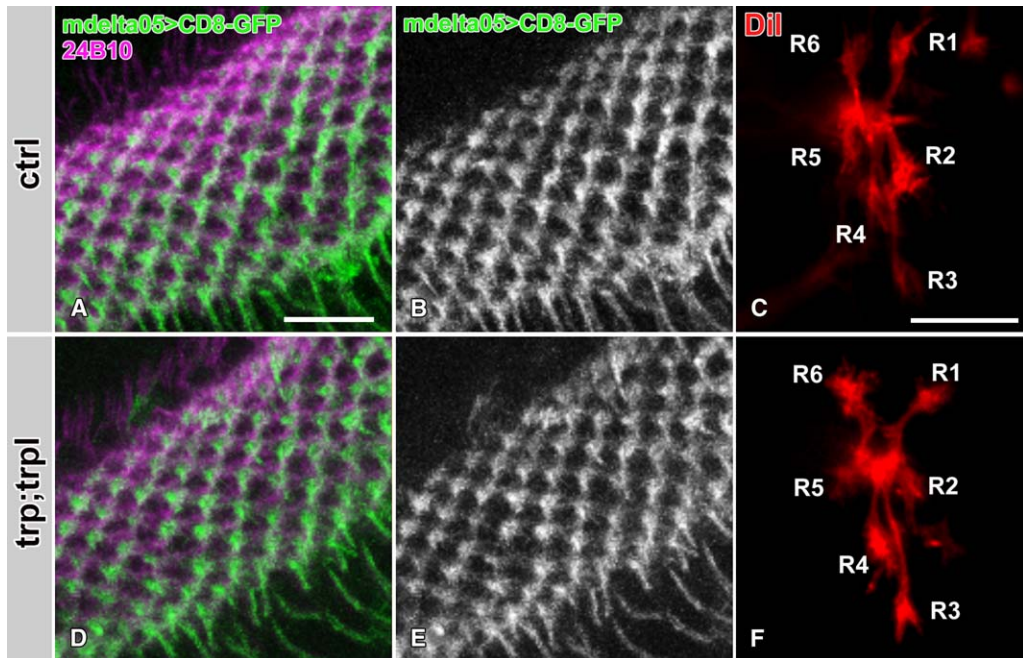


Figure S3. Photoreceptor Subtype-Specific Targeting in *trp;trpl* Mutants

(A and B) R4-specific labeling of the developing lamina plexus in wild-type. Green, *mdelta0.5* driven CD8-GFP; magenta, 24B10 [S10].

(D and E) R4-specific labeling as in (A) and (B) for *trp³⁴³;trpl³⁰²* [S7].

(C and F) Dll-injected axons from single ommatidia as described in [S14]. (C) Wild-type; (F) *trp³⁴³;trpl³⁰²* [S7]. The faint process underneath R2 in this panel is from a weakly labeled axon in a neighboring ommatidium.

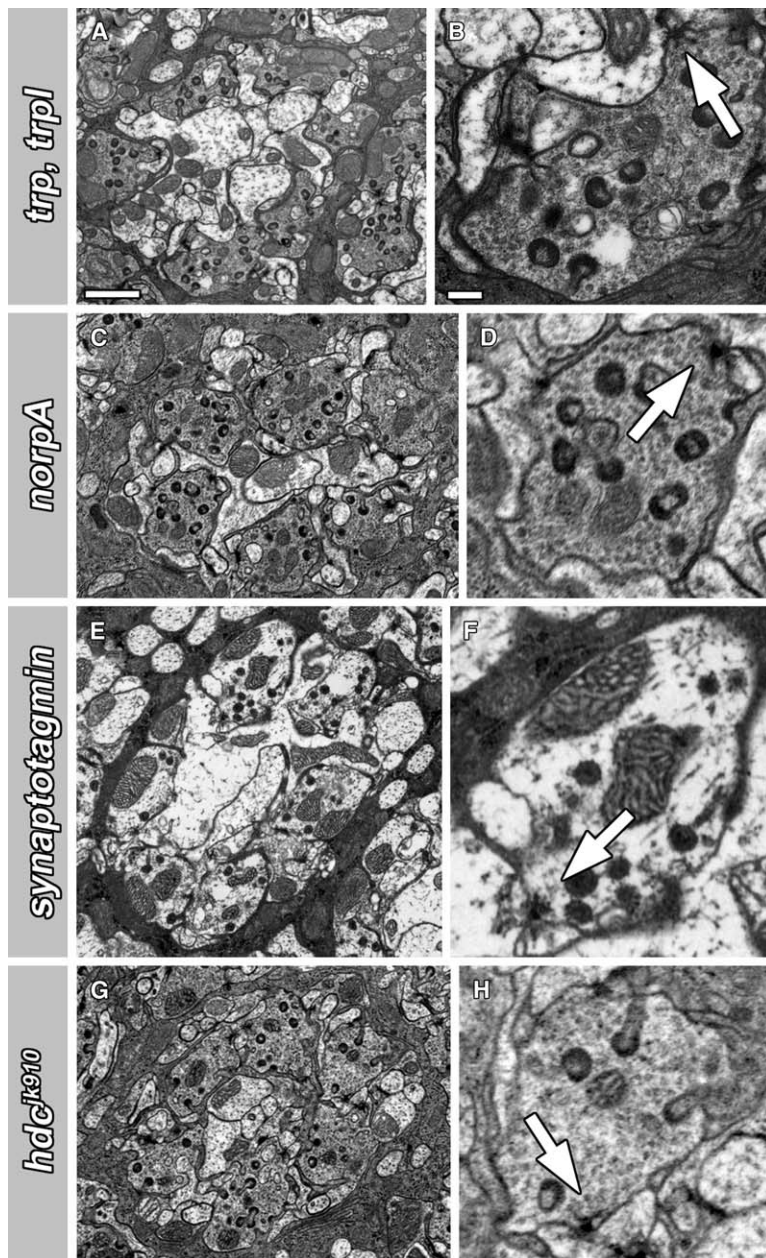


Figure S4. Ultrastructural Investigation of Activity Mutants

(A and B) EM micrographs of lamina cross-sections of *trp³⁴³;trpl³⁰²*. (C and D) *norpA^{p24}*. (E and F) *synaptotagmin^{AD4}*. (G and H) *hdc^{k910}*. Synapses are marked with arrows. Scale bars in (A) represent 1 μ m for (A), (C), (E), (G) and in (B) represent 200 nm for (B), (D), (F), (H).

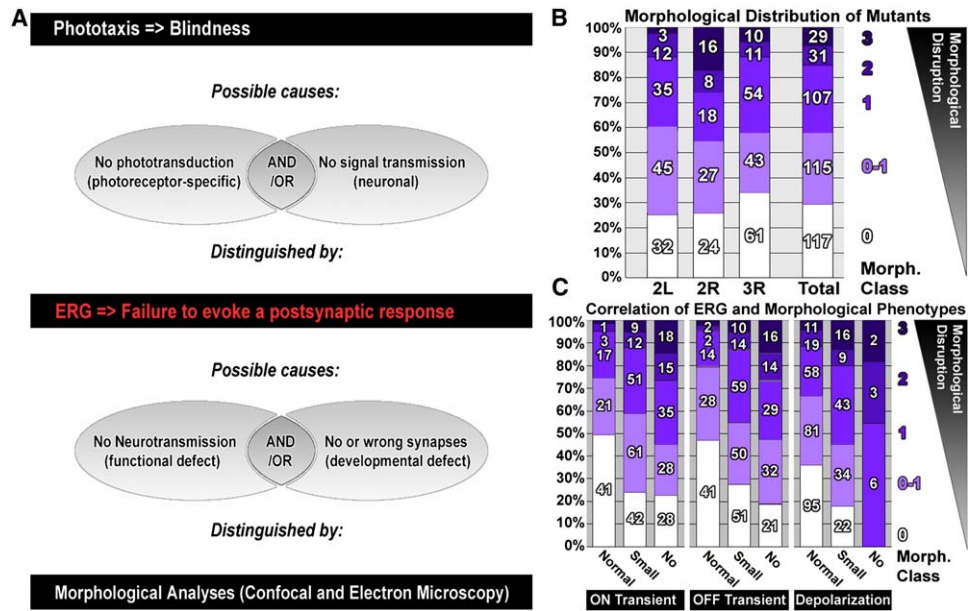


Figure S5. A Forward Genetic Screen for Mutants that Fail to Evoke a Postsynaptic Response in the Visual System of the Fly

(A) Flowchart of the screen design of the eyFLP [S4] screen as previously reported [S11, S15].

(B) Distribution of mutants in different morphological classes (cf. Figure S6) for the separately screened chromosome arms 2L, 2R, and 3R. Bars represent percentages; numbers in bars actual number of mutants.

(C) Correlation of electroretinogram (ERG) and morphological classes. Mutants with stronger phenotypes in the ERG (no on transient, no off transient, no depolarization) are more often morphologically disrupted than those with weaker ERG phenotypes, indicating that selection of stronger ERG phenotypes enriched for stronger morphological phenotypes.

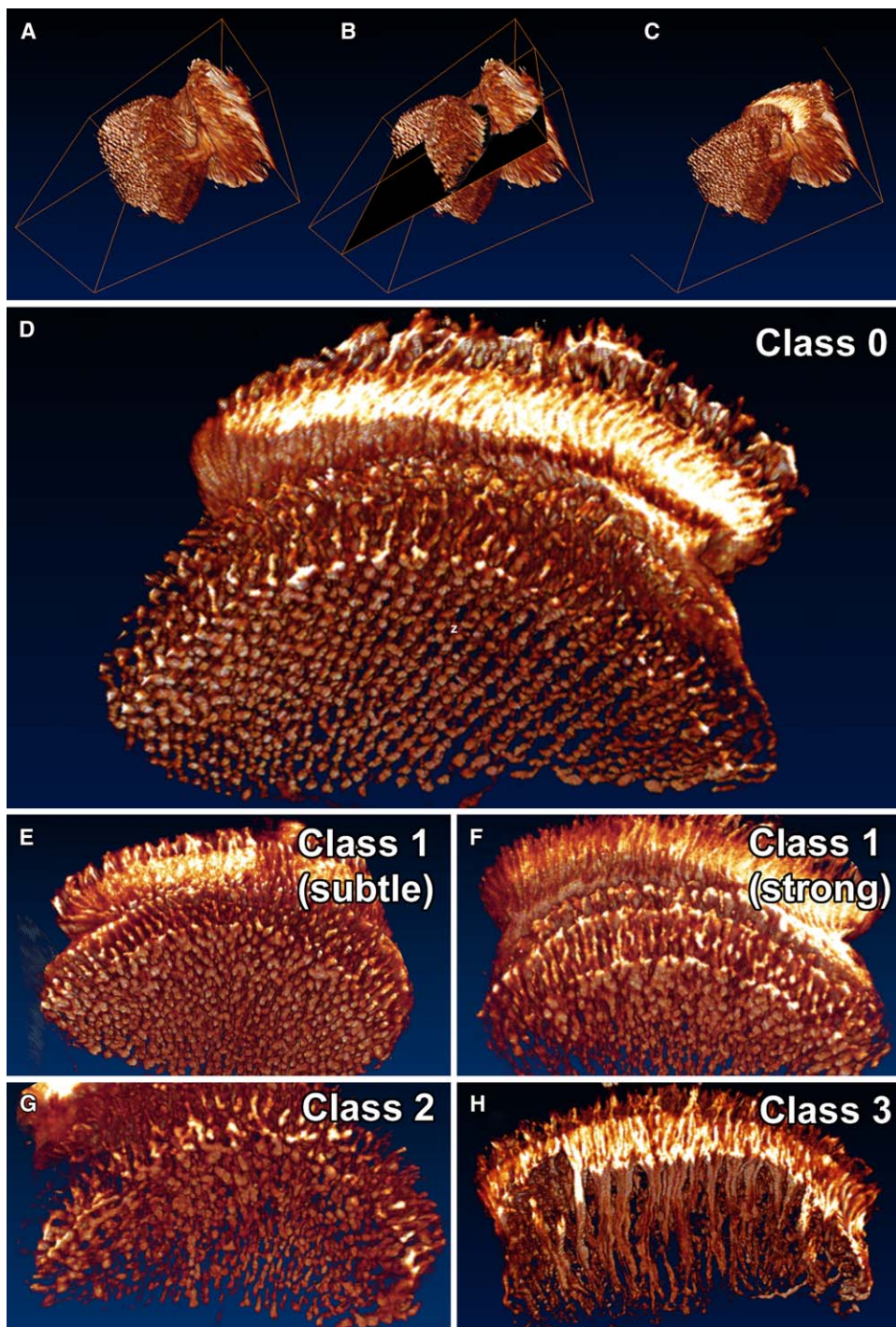


Figure S6. Classification of Morphological Mutants Isolated in the Screen Based on 3D Visualization of Photoreceptor Projections

Brains were dissected and stained with the photoreceptor-specific antibody mAb 24B10 [S10].

(A–D) Semiautomated confocal scans were analyzed by real-time volume rendering as depicted in (A) horizontal view of the photoreceptor projections, (B) application of a cutting plane, (C) removal of the dorsal half of the projection field, (D) view from inside the brain into the cut lamina, R7/8 medulla projections, and R7 terminal field (cf. Figure 1B).

(E) Example of a class I morphological mutant selected for a subtle R7 terminal pattern disruption due to terminal fusions.

(F) Example of a strong class I morphological mutant selected for abundant R7 terminal fusions.

(G) Example of a class II morphological mutant; note the loss of the R7/8 layer distinction in the medulla.

(H) Example of a class III (pathfinding) mutant. Note the aberrant axon bundles.

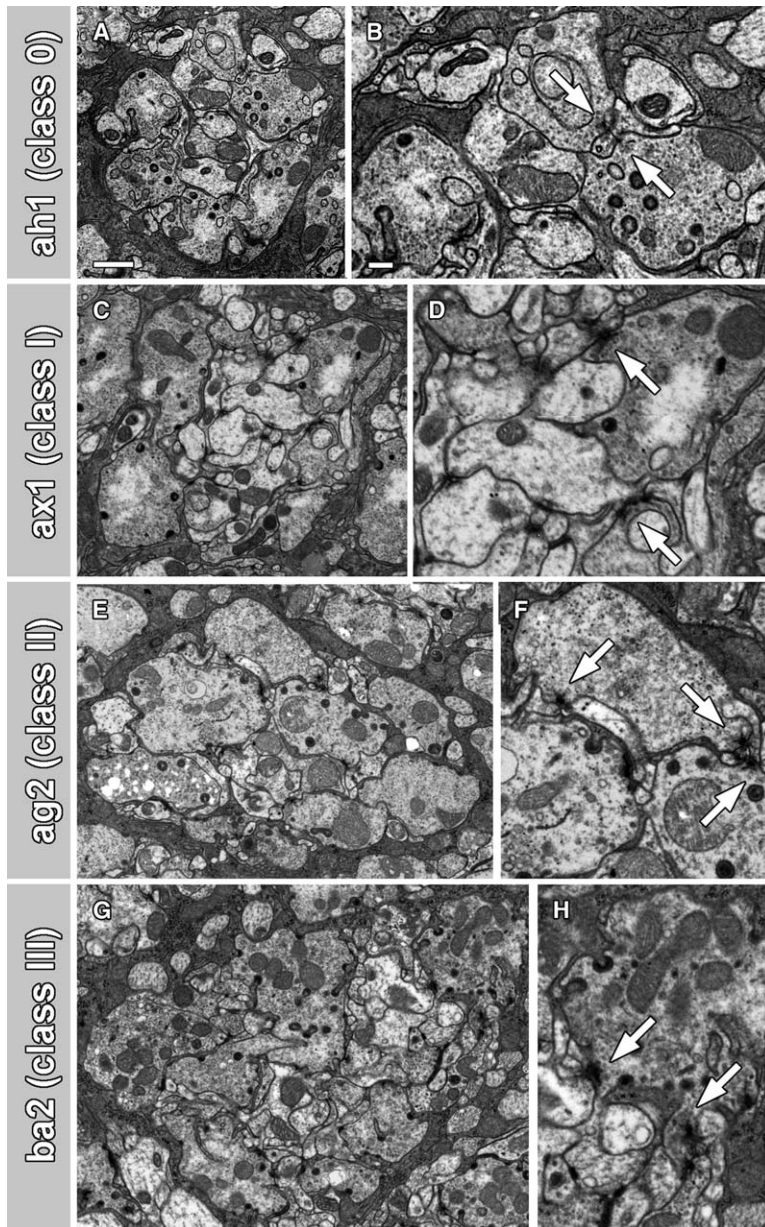


Figure S7. Examples of 4 out of 60 Mutants Analyzed with Quantitative Electron Microscopy

(A and B) Class I mutant (ah1).

(C and D) Class I mutant (ax1).

(E and F) Class II mutant (ag2).

(G and H) Class III mutant (ba2). Synapses are marked with arrows. Scale bars in (A) represent 1 μ m for (A), (C), (E), (G) and in (B) represent 200 nm for (B), (D), (F), (H).

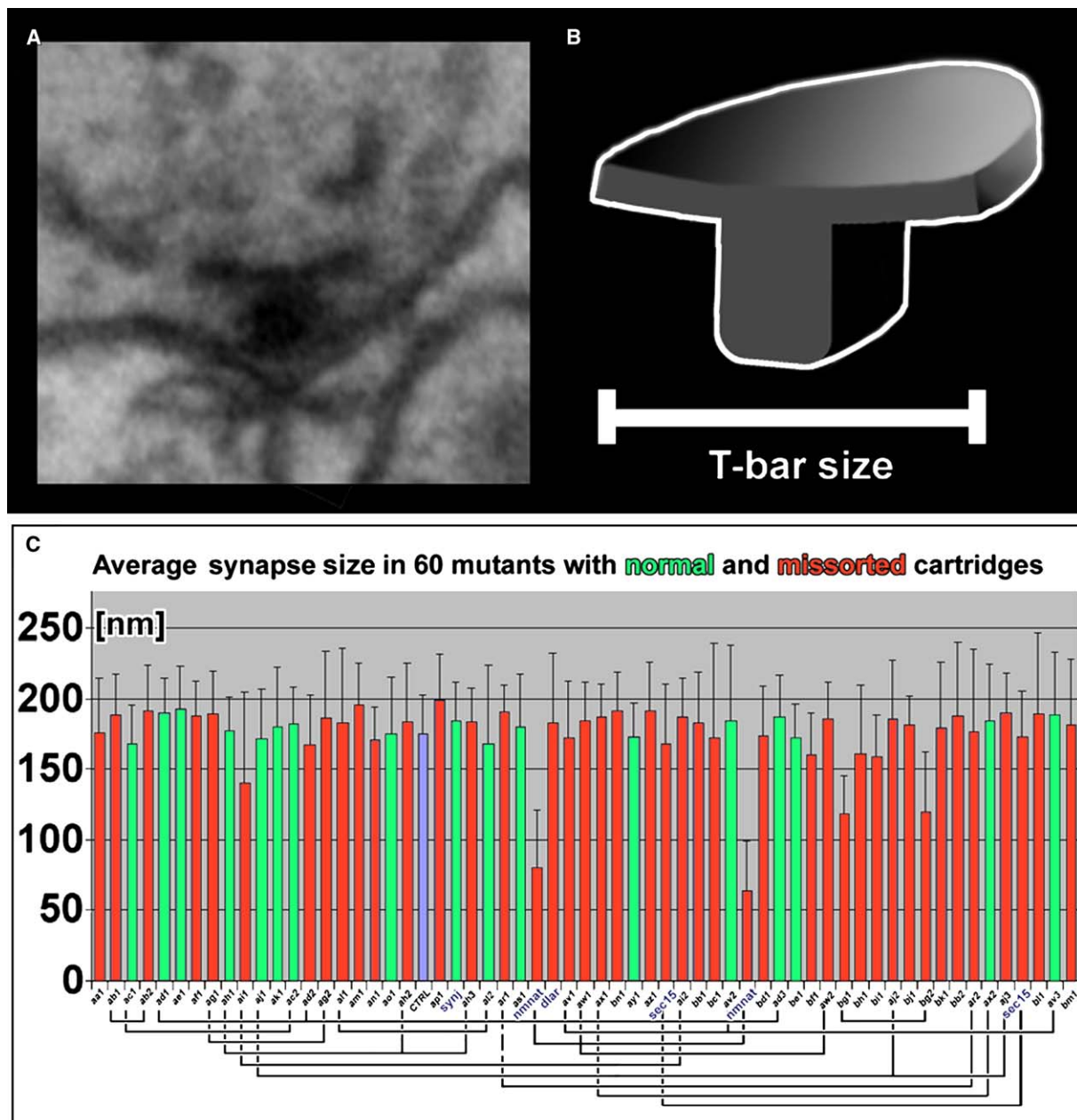


Figure S8. Morphological Analysis of Synaptic Profile Size in All Mutants

(A) TEM micrograph of a wild-type synaptic profile, showing a cross-section of the presynaptic T-bar.

(B) Cartoon of a cross-section of a T-bar. Only cross-sections of T-bars were quantified. However, since the platform of the T-bar is longer in length than in width, small differences in section angles lead to a normally observed variation of 150–250 nm.

(C) Quantification of T-bar cross-sections lengths in all mutants (same order as Figure 3A). Control is shown in blue. Alleles of the same complementation groups are marked by connecting lines underneath the x axis.

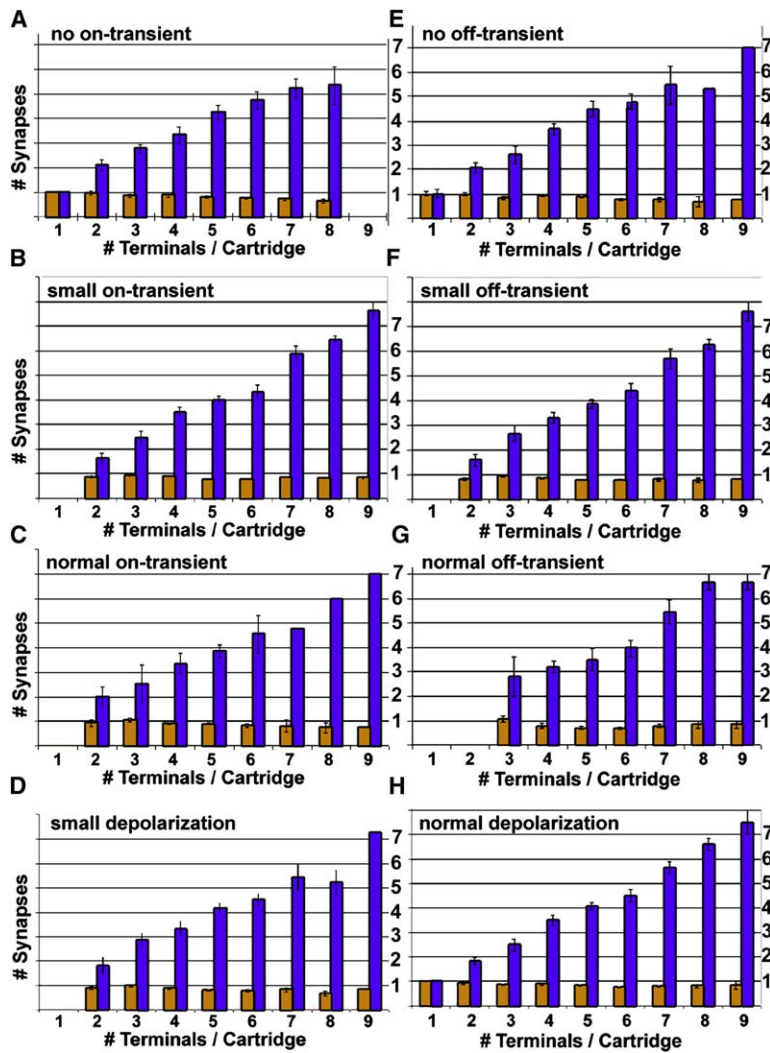


Figure S9. Synapse Numbers per Photoreceptor Terminal as a Function of Cartridge Composition in Different Groups of Electroretinogram Mutants

The number of synapses per terminal is shown in orange, and no significant difference was observed among different cartridge compositions. The number of synapses per cartridge is shown in purple. All cases are in perfect agreement with model A shown in Figure 4A.

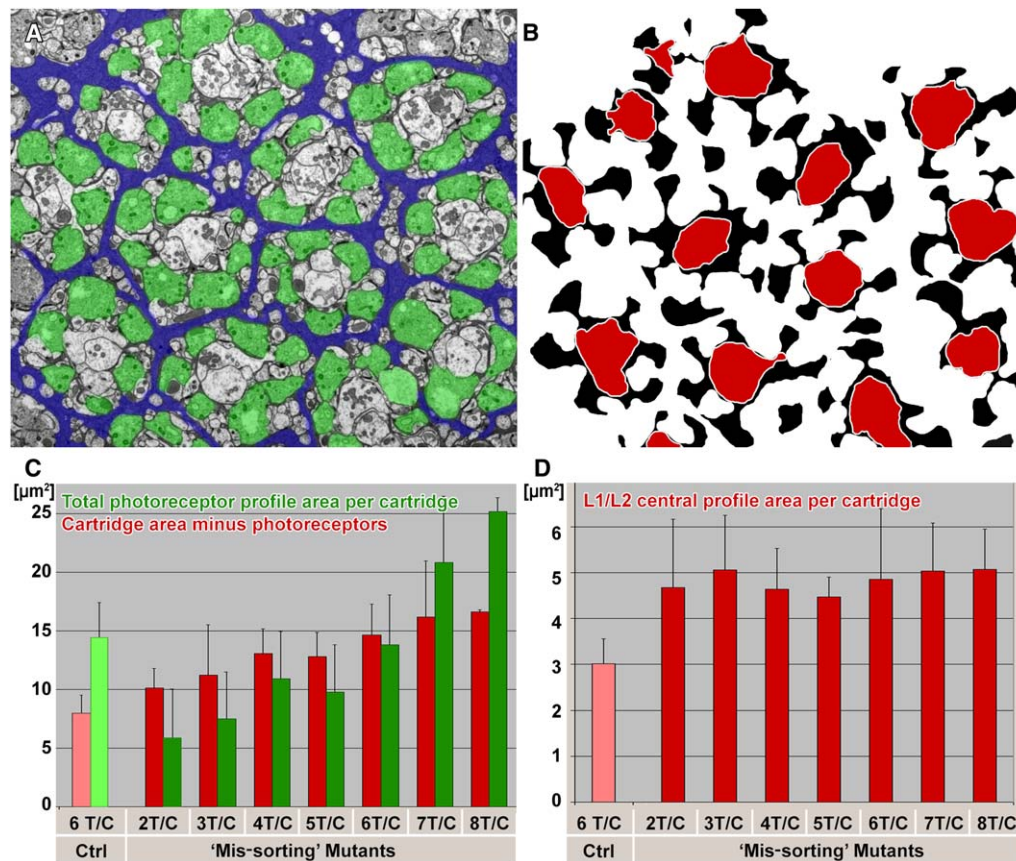


Figure S10. Quantification of Postsynaptic Profiles in Cartridges with Varying Photoreceptor Terminal Complement

(A) EM of a lamina cross-section of a mutant with varying photoreceptor terminal numbers per cartridge, but clearly discernible cartridge structure and central L1/L2 profiles.

(B) Quantification of postsynaptic profiles. The black areas demarcate manually labeled complete cartridges from which all recognizable photoreceptor terminals and obvious glial processes have been subtracted. The red areas demarcate clearly discernible central L1/L2 profiles.

(C) Total area (in μm^2) of the total photoreceptor profile area per cartridge (green) and cartridge area minus photoreceptors and obvious glial processes (red) in all missorting mutants with discernible cartridge boundaries as a function of the number of terminals per cartridge (e.g., black areas in [B]).

(D) Total area (in μm^2) of the central L1/L2 profiles per cartridge in missorting mutants with discernible boundaries and cartridge organization that allows the clear distinction of these central profiles (e.g., red areas in [B]).